Efficiency of hanging silt curtains in cross-flow

Max Radermacher[1], Lynyrd de Wit[2], Johan C. Winterwerp[3], Wim S.J. Uijttewaal[4]

Abstract

When dredging in sensitive environments, efforts have to be made to limit the free dispersal of suspended fine sediment from the dredging spill. Especially the use of hanging silt curtains as an environmental mitigation measure is widespread. Despite frequent application, their ability to reduce turbidity levels through vertical diversion of sediment-laden currents remains subject of debate. This paper addresses a series of laboratory measurements and numerical model simulations in order to determine the efficiency of hanging silt curtains, defining a new efficiency parameter. The model was validated against the laboratory experiments. Model simulations focusing on vertical diversion of the sediment-laden current suggest that hanging silt curtains do not have a favorable influence on the settling of suspended sediment when applied in cross-flow. Diversion of currents underneath the curtain causes flow separation and intense turbulent mixing, which counteracts settling of suspended sediment particles. The results imply that the widespread application of hanging silt curtains should be reconsidered from a physical point of view.

ASCE Subject headings: Dredging, Turbidity, Environmental issues, Turbulence, Numerical models, Laboratory tests

[1] Ph.D. Student, Delft Univ. of Technology, Faculty of Civil Engineering and Geosciences, Stevinweg 1, 2628CN Delft, The Netherlands (corresponding author). E-mail: m.radermacher@tudelft.nl.
[2] Fluid Mechanics Expert, Svasek Hydraulics, Schiehaven 13G, 3024EC Rotterdam, The Netherlands.
[3] Professor of Sediment Dynamics, Delft Univ. of Technology, Faculty of Civil Engineering and Geosciences; and Senior Expert, Deltares, Rotterdamseweg 185, 2629HD, Delft, The Netherlands.
[4] Professor of Experimental Hydraulics, Delft Univ. of Technology, Faculty of Civil Engineering and Geosciences, Stevinweg 1, 2628CN Delft, The Netherlands.

Introduction

During several stages of a dredging cycle, fine sediment may be released in the water column. Owing to its low settling velocity, fine sediment can stay in suspension for long periods of time. The resulting turbidity clouds, subject to ambient currents, are transported away from the dredging site. This elevated turbidity may have an adverse effect on primary production rates and various vulnerable marine species, corals and sea grasses being notorious examples (Bray 2008; Erftemeijer and Robin Lewis 2006; Erftemeijer et al. 2012). Shading (i.e. attenuation of daylight) and burial are the main processes responsible for this possible environmental impact.

In order to protect the marine environment, dredging contractors and their clients take environmental mitigation measures when necessary. Application of silt curtains is often regarded an efficient way to avoid dispersal of suspended fine sediment. Silt curtains are flexible barriers, deployed between the source of turbidity and a sensitive receptor. They come in two basic types, being the hanging and the standing type, see Figure 1. Hanging silt curtains consist of a series of floaters on the water surface and a flexible cloth, which is kept more or less vertical by heavy chains. A gap is maintained near the bed to account for tidal modulation and pressure release in case of cross currents, which also leads to flaring of the curtain. At many dredging projects worldwide, hanging silt curtains are placed in cross-flow. In that case, the intended working principle of the curtain is to divert the current vertically through the gap between the curtain and the bed. This is assumed to reduce the settling time of suspended sediment which is transported with the cross-flow, diverting the current towards the bed. Standing curtains are attached to a heavy sinker pipe near the bed and a series of floaters on the free surface, typically covering the full water depth. Because a pressure release mechanism is lacking, standing curtains are more sensitive to mechanical failure when placed in a cross-flow. Hence, their intended working principle differs from that of hanging silt curtains. Standing curtains are generally used to separate the source area of turbidity from the main flow and create a calm zone, which is not always feasible, depending on the intensity of environmental conditions. Furthermore, they require heavy floating equipment for (re)placement. As a result, many dredging contractors have a preference for the hanging type. In this paper, the focus is on hanging silt curtains in cross-flow. Also, the case of applying silt curtains directly in front of a sensitive receptor, so as to guide suspended sediment away from the sensitive environment, is disregarded in this study.

Silt curtains can be placed in various configurations, depending on the requirements and constraints of the dredging project (Francingues and Palermo 2005). The schematic in Figure 2 shows two representative configurations for hanging silt curtains. Configuration (a), the open configuration, is typically applied at some distance from the shore, when the spatial scale of the dredging site is large and accessibility must be guaranteed. Configuration (b) is situated at the open end of a semi-enclosed reclamation area.

This paper assesses the efficiency of hanging silt curtains when subject to an ambient cross current of arbitrary, but significant flow velocity. That situation applies for example to configuration (a), but also to configuration (b) in case of an ebb-tidal current or a wind-driven current when the semi-enclosed basin is of considerable size. In this study, the case of cross-flow passing a hanging silt curtain is treated as a two-dimensional vertical (2DV) flow problem in a transect perpendicular to the curtain. By doing so, lateral effects like horizontal diversion of flow are ignored. The consequences of this approach are limited and do not obscure the analysis of silt curtain effectiveness, as treated in further detail in the discussion section.

Hanging silt curtains are supposed to divert sediment-laden currents towards the bed, thereby reducing the time to settle from the water column and the horizontal range of influence of the suspended sediment. However, based on practical experience, questions have been raised on the efficiency of hanging silt curtains (Francingues and Palermo 2005, Vu and Tan 2010, Ogilvie et al. 2012). In particular, vertical mixing downstream of the silt curtain is often observed to counteract the settling induced by the curtain.

Scientific research into silt curtain efficiency, as published in literature, has not addressed the topic to its full extent yet. The main focus has been on mechanical and practical aspects of silt curtains (JBF Scientific Corporation 1978; Francingues and Palermo 2005; Ogilvie et al. 2012). The efficiency of silt curtains as an environmental mitigation measure has been treated by Yasui et al. (1999), Jin et al. (2003), Vu et al. (2010), Vu and Tan (2013) and Wang et al. (2015), based on laboratory experiments and measurements in the field. The painstaking nature of such physical model tests has inhibited rigid conclusions regarding the effect of silt curtains on the reduction of turbidity under various relevant conditions. Hanging silt curtain efficiency reported from field measurements varies from slightly favorable (Vu et al. 2010) to explicitly unfavorable (Jin et al. 2003), based on sparse measurements. The complexity of the flow field around a silt curtain and the use of different measurement locations and analysis methods hamper interpretation and comparison of the results. Therefore a combination of laboratory tests and advanced numerical modeling seems attractive.

This study aims at assessing the efficiency of silt curtains under the relevant range of flow conditions one may encounter in cases of silt curtain application. To this end, use is made of numerical model simulations, which yields an extensive dataset suitable for sensitivity analysis. Validation of the numerical model results is done by comparing to physical model experiments. Both models and their comparison are described in the modeling section, including upscaling of the numerical model from laboratory scale to full scale. Subsequently, the parameters which should be used to quantify the efficiency of silt curtains are introduced. In the results section, the results of the numerical model simulations, including suspended sediment transport, are presented and silt curtain efficiency is evaluated. Some additional aspects of the results are treated in the discussion section, followed by the conclusions.

Modeling

The turbulent flow field and sediment concentrations around a silt curtain were assessed using a laterally non-varying approach. In the 3D physical and numerical models which were employed, the silt curtain covered the full width. Lateral diversion of flow around the edges of a silt curtain is not possible with this approach, hence the full fine sediment flux is forced to pass underneath the curtain. The implications of this choice are discussed in further detail in the discussion section. A numerical model, based on Large Eddy Simulation, was used to assess the efficiency of silt curtains at full scale. First, the model setup is treated. Physical experiments in a laboratory flume were conducted to validate the computed turbulent flow field at laboratory scale, at Froude numbers which are close to realistic conditions in the field. Next, the experimental setup and visual observations of the flow field are described and finally the validation is presented.

Numerical model

In the flow field around a silt curtain, flow separation and turbulent mixing play a prominent role. Reliable results are only expected when the turbulent flow field is (partly) resolved, which is done in this study through the application of Large Eddy Simulation (LES). In this type of turbulence modeling, turbulent fluctuations are averaged over every numerical grid cell (i.e. averaged in space), in contrast to the more conventional Reynolds averaged (i.e. ensemble averaged) approach. LES allows turbulent vortices to develop down to the scale of the computational mesh size. At the upstream boundary, turbulent eddies were seeded through the use of the synthetic eddy method (SEM; Jarrin et al. 2006). The time-averaged flow velocity profile at the upstream boundary was logarithmic.

Although the flow problem assessed in this laterally non-varying approach is essentially 2DV, the application of LES made a 3D model domain necessary. Turbulence behaves fundamentally different in a 2DV domain than in a 3D domain, as vortex stretching cannot be accounted for adequately in two dimensions (e.g. Kraichnan and Montgomery 1980). Hence a third dimension was added to the numerical model domain, with a length scale similar to the water depth. The computational grid consisted of 450x40x40 cells in the x, y and z direction respectively. The silt curtain covered the full width of the domain and was represented as a vertical, stiff and straight baffle, see Figure 3. The actual, flared shape of the curtain as encountered in reality was not included in the model directly, although the height of the baffle was adjusted to the effective height after flaring as measured in the laboratory. At sub-grid level, turbulent diffusion was represented by the wall-adapting local eddy-viscosity (WALE) model (Nicoud and Ducros 1999). Erosion of the bed was not included in the model, as to avoid confusion of different processes influencing turbidity levels around the silt curtain. A detailed description of the model is included in the appendix.

Physical model

Validation of these turbulent flow simulations requires high-frequency velocity measurements in a laboratory flume. To this end, Laser Doppler Anemometry (LDA) was applied in the laboratory set-up presented in Figure 4. The flow velocity was sampled at 100 Hz for 200 s in a 6 x 19 grid (x and y directions respectively) downstream of a silt curtain scale model. The flume had a width of 0.40 m and a length of 14 m. The discharge was controlled by a valve in the supply pipe and measured by means of a digital flow meter. The water depth was controlled by a weir at the downstream end of the flume, and was kept fixed at 0.35 m.

The physical experiment covered a series of six different conditions, varying both the relative silt curtain height h_{rel} and the Froude number F, see equations 1 and 2. Here, h_s is the effective silt curtain height after flaring (see Figure 5), h represents the water depth, U represents the depth-averaged flow velocity along the x-coordinate and g denotes the gravitational acceleration.

$$h_{rel} = \frac{h_s}{h} \tag{1}$$

$$F = \frac{U}{\sqrt{gh}} \tag{2}$$

$$R = \frac{Uh}{\nu} \tag{3}$$

Values of F, ranging from 0.029 to 0.071, were chosen for representing realistic conditions in the field ($h = 5$ m and $U = 0.2 - 0.5$ m/s). As a result, the Reynolds number R (see equation 3, where ν is the kinematic viscosity) attained significantly lower values in the laboratory ($1.7 \cdot 10^4$ – $4.2 \cdot 10^4$) than in the field ($9.1 \cdot 10^5$ – $2.3 \cdot 10^6$). However, these Reynolds numbers fall within the turbulent regime. Combined with the strong silt curtain-induced flow disturbance, turbulent flow should fully develop at laboratory scale.

During the physical experiments, use was made of a flexible silt curtain with weights attached at its lower edge. As in reality, this led to flaring of the silt curtain when exposed to a cross current. A weighting of 1.24 kg/m was chosen in order to achieve realistic curtain deformations under the tested range of Froude numbers. Before flaring, the two different curtains applied in the experiments had relative curtain heights of 0.5 and 0.75 (i.e. the curtains covered 50% and 75% of the water depth, respectively). The relative curtain height after flaring was variable, depending on the flow rate in the flume and the associated deformation of the curtain. The silt curtain scale model was constructed from a flexible, densely woven fabric. No attention was paid to details of the fabric's permeability, but visualizations with dye showed that virtually no water passed through the fabric. The gap between the curtain and the bed provides a far more effective pressure release in case of a cross current than possible permeability of the fabric would. The flow, seeking for the path of least resistance, passes underneath the curtain rather than through. This effect was verified using dye injections and is expected to occur in the field as well. Clogging of the fabric and marine growth on the silt curtain add to this behavior.

The turbulent flow field observed in the laboratory was visualized with dye, see Figure 5. The curtain causes flow separation, leading to wake formation and strong production of turbulence. Vortices grow from the curtain's lower edge and transport dye upward. Most of the dye is advected downstream with the main flow, but part of the dye gets trapped in the wake and is gradually reintroduced in the main flow. Although turbulent mixing appears to be less intense for lower F and h_{rel}, the flow field described above remains qualitatively the same for all configurations.

Validation of numerical model

Two steps are presented to arrive at a suitable full scale numerical model. First, flow parameters as computed with a laboratory-scale numerical model are validated by comparing them to flow parameters which were measured during the laboratory experiment, using the same boundary conditions. The second step comprises of comparing full scale computations to laboratory scale computations.

Figure 6 shows computed and measured time-averaged horizontal and vertical flow velocities along the central axis of the model domain for $h_{rel} = 0.5$ and $F = 0.043$ as an example. Similar results and performance are found for all other tested configurations. The profiles of time-averaged horizontal flow velocity $\overline{u}$ show a near-bed jet flow induced underneath the silt curtain. Flow separation leads to the formation of a recirculation zone in the upper half of the water column, indicated in the upper panel. The dashed line marks the region where the time-averaged horizontal flow velocity integrates to zero along the vertical dimension, i.e. the mean dividing streamline. Further downstream, the jet flow spreads over the full water depth, which is associated with a redistribution of momentum through upward mean flow velocities (positive $\overline{w}$) in this region. Generally, the numerical model closely follows the laboratory experiments, given root-mean-square (RMS) errors of 5% for the horizontal velocity and 25% for the vertical velocity, relative to the maximum value measured in the second vertical profile ($x = 0.4$ m) .

A comparison of turbulence parameters is presented in Figure 7. Turbulence intensity is defined here as the standard deviation of the velocity time series. Flow separation near the lower edge of the silt curtain causes peak values of all turbulence parameters in this region, which diffuse over the full water column further downstream. The Reynolds shear stress τ_{uw}, shown in the lower panel, is a measure for turbulent transport of dissolved or suspended matter. These profiles express intense turbulent mixing along the wake induced by the silt curtain. The performance of the LES model is good, as RMS errors remain very small (11% for horizontal turbulence intensity r_u, 11% for vertical turbulence intensity r_w and 10% for τ_{uw}, relative to the maximum values measured in the second vertical profile).

Next to this sequence of vertical profiles of flow parameters, the laboratory and numerical results are compared in the frequency domain. Figure 8 shows the one-dimensional frequency spectra of turbulent kinetic energy as derived for the experiment presented in Figures 6 and 7 ($h_{rel} = 0.5$ and $F = 0.043$) at half depth and $3.5h$ downstream of the silt curtain. The figure also distinguishes between the macro scale and the inertial range with a $f^{-5/3}$ scaling (Pope 2000). An important requirement for the LES approach to be valid, is isotropy of turbulence at the sub-grid scales. This requirement appears to be fulfilled, since the spectrum derived from the numerical model partly covers the inertial range before being cut off by mesh size limitations at higher frequencies.

Hence, it can be concluded that the ability of the LES model to simulate the flow field around a silt curtain has been demonstrated at laboratory-scale ($h = 0.35$ m). However, silt curtain efficiency is determined from numerical simulations at full scale ($h = 5$ m). The flow field is dominated by free turbulence, as a result of flow separation at the tip of the silt curtain. Such a flow field is known to depict self-similarity when scaled with F and the governing geometric parameter (in this case h_{rel}), while hardly depending on the Reynolds number. Therefore, the profiles of flow and turbulence parameters for full scale simulations are similar to those shown in Figures 6 and 7, with peak values at the same relative depth (z/h), but of different magnitude, depending on the Froude-scaling. Hence, it is argued that upscaling of the model results to realistic length scales does not introduce any significant error.

It was indicated that the curtain is represented in the numerical model as a vertical, straight baffle, without the possibility to deform under influence of a cross current, but with the correct curtain height after flaring. However, through the formation of an eddy near the surface upstream of the baffle (see Vu and Tan, 2010), the main flow attains a shape as if it were deflected by a flared silt curtain. The orientation of the streamlines around the tip of the curtain in the numerical model closely resembles those in the physical model. This makes the amount of flow contraction in the jet flow very similar for both models. Hence, from the positive validation presented in this section, the consequences of this simplification appear to be limited, although it might explain the occurrence of some small deviations.

Silt curtain efficiency is determined from suspended load transport calculations of fine sediment. Down to the mesh size, advection of suspended sediment by turbulent motions (i.e. turbulent diffusion) is captured by the LES approach. The sub-grid-scale diffusion coefficient Γ is obtained from the eddy viscosity ν_e by dividing the latter by the turbulent Prandtl-

Schmidt number, Sc. Antonopoulos-Domis (1981) demonstrates that $Sc = 0.5$ is appropriate for fitting LES computations to laboratory data of isotropic turbulence. This finding is adopted here. Moreover, we found that the sensitivity of the advection-dominated LES model to Sc is very small (differences in suspended sediment concentrations for model simulations with $Sc = 0.4$ and $Sc = 1.0$ are generally very small throughout the whole domain; the maximum deviation computed is 1% of the uniform concentration at model inflow). This provides further proof of the fact that sub-grid diffusion only has minor influence on sediment transport in the present model and that this model therefore is well capable of resolving turbulent mixing around the silt curtain. The suspended sediment concentrations used in this study (< 100 mg/L) are far too low to have an influence on hydrodynamics through e.g. density differences (Whitehouse et al., 2000). Further validation of the suspended sediment transport model has been carried out by De Wit (2015).

Efficiency parameters

Before the model results can be discussed, appropriate parameters should be defined for quantification of silt curtain efficiency. Various authors have proposed a comparison of representative downstream and upstream values of suspended sediment concentration C for this purpose (JBF Scientific Corporation 1978; Francingues and Palermo 2005; Vu et al. 2010; Ogilvie et al. 2012). This approach is disputable because of two reasons. First, C does not fully express the possible environmental impact posed by turbidity. In general, suspended particles near the water surface have a much larger settling time than suspended particles near the bed, and can therefore be transported further away from the source (in this case the dredging site). Moreover, particles near the surface have a larger influence on the light climate in the water column than particles near the bed. Second, comparing downstream values to upstream values does not only express the influence of the silt curtain on turbidity values. It also reflects 'undisturbed' settling of the sediment between the two locations, defined here as settling of individual particles under influence of their settling velocity rather than downward advection by the flow. Especially for relatively coarse sediment and low ambient flow velocities, this must play a significant role.

The first problem is resolved by introducing an environmental impact potential P, as defined in equation 4, in which lateral variations (y coordinate) are neglected. The linear dependency on C in this equation can be justified with data from Erftemeijer and Robin-Lewis (2006) and Erftemeijer et al. (2012), which show an approximately linear relation between suspended sediment concentrations and the environmental damage done to exposed corals and sea grasses, respectively. The influence of the vertical concentration distribution is incorporated by multiplying C with the vertical coordinate z. With $z = 0$ at the bed, the highest impact potential is assigned to suspended sediment near the free surface. Integration over the water column results in a longitudinal distribution of the environmental impact potential P, which is essentially the first moment of the vertical concentration distribution.

$$P(x) = \int_0^1 z_* C_* \left(x,z\right) \mathrm{d}z_* \qquad (4)$$

with:

$$z_* = \frac{z}{h}$$
$$C_* \left(x,z\right) = \frac{C(x,z)}{C_{\max}}$$

Here, z and C are made dimensionless with the water depth h and the maximum concentration at model inflow $C_{\max}$, yielding z_* and C_*.

The second problem is resolved by introducing an efficiency parameter, expressing the reduction in P. As mentioned before, several authors have compared downstream values to upstream (i.e. at inflow of the model domain) values. This yields the gross silt curtain efficiency E_S as defined in equation 5, whereas we prefer to use the environmental impact potential P, instead of C.

$$E_S\left(x\right)=\frac{P_{in}-P\left(x\right)}{P_{in}}\cdot 100\% \qquad (5)$$

As discussed, undisturbed settling of suspended sediment, which would also occur in conditions without a silt curtain, should be excluded from the efficiency parameter. This can be done through a reduction accounting for the settling of particles without a curtain. Thus, the reference value $P_{ref}\left(x\right)$ is obtained from a reference simulation without a silt curtain, which is substituted into equation 5 to obtain the reference efficiency $E_{ref}\left(x\right)$. Reduction of $E_S\left(x\right)$ with $E_{ref}\left(x\right)$ yields the net silt curtain efficiency $E_{net}\left(x\right)$, see equation 6.

$$E_{net}\left(x\right)=E_S\left(x\right)-E_{ref}\left(x\right)=\frac{P_{ref}\left(x\right)-P\left(x\right)}{P_{in}}\cdot 100\% \qquad (6)$$

The difference between both parameters is illustrated with the conceptual example in Figure 9. This figure shows an initially depth-uniform concentration field in a flow with (upper panel) and without (lower panel) a silt curtain. Initially, the silt curtain brings the suspended sediment closer to the bed. However, strong turbulent mixing in the wake induces an upward flux of sediment, re-establishing the approximately uniform concentration profile over depth.

In the flow field without a silt curtain, persistent settling gradually brings the sediment grains towards the bed. Values of P, indicated above every concentration profile in this figure, show that the silt curtain achieves a 30% reduction in the environmental impact potential (i.e. from $P = 0.5$ to $P = 0.34$). In the conventional view of silt curtain efficiency, the curtain has a favorable influence on turbidity levels, which is reflected by the gross efficiency: $E_S = 32\%$. However, if the curtain is absent, the reduction of P is about 40%, as a result of undisturbed settling. Hence the net effect of the curtain is unfavorable, which is reflected by the net efficiency: $E_{net} = -10\%$. This example expresses the difference between both efficiency parameters. E_S represents the combined effect of the silt curtain and undisturbed settling, whereas E_{net} merely contains the effect of the curtain.

In this study, $x = 10h_s$ was adopted as the distance downstream from the curtain where P and the efficiency parameters are evaluated. The region immediately downstream of the curtain is dominated by turbulent mixing, whereas settling of the sediment gradually takes over further downstream. The horizontal extent of the recirculation zone is found to be between 6 and 7 times the silt curtain height in our simulations. In order to evaluate silt curtain efficiency at the same position relative to the flow field in every simulation, h_s is used to determine the evaluation coordinate. The position where vertical flow profiles reach their undisturbed values again is situated much further downstream, outside the model domain. To be as close as possible to this location, the maximum multiple of h_s that fits inside the model domain for all simulations was chosen, being $x = 10h_s$. Further downstream (i.e. outside the model domain), the presence of the curtain will mainly have some unfavorable impact through elevated turbulence levels and mean upward velocities due to vertical redistribution of momentum. Although turbulent shear stresses and upward flow velocities in that region are one order smaller than inside the recirculation zone, it is expected that efficiency values presented in this study have a small, positive bias. They should be interpreted as an upper limit of silt curtain efficiency.

Results

Next, the LES model is used to generate an extensive dataset. Throughout the simulations, three parameters are varied, being the relative curtain height h_{rel} (see equation 1), the velocity ratio θ (see equation 7, w_s denotes the settling velocity of the sediment particles) and the suspended sediment concentration profile at model inflow (see Figure 10), upstream of the silt curtain.

$$\theta = \frac{w_s}{U} \qquad (7)$$

The range of tested parameter values is presented in Table 1. The water depth is fixed, whereas the silt curtain height is varied. This choice does not constrain the validity of this study, as the flow field is controlled by the ratio of curtain height versus water depth. By varying h_s and keeping h fixed, the findings are valid for values of h_{rel} between 0.25 and 0.75. Smaller values would lead to negligibly short silt curtains, whereas larger values do hardly occur in practice due to flaring of the curtain. Only with the application of very heavy weight chains, larger relative curtain heights are achievable, but this drastically increases the forces acting on the curtain with the risk of mechanical failure. Tested ambient flow velocities range between 0.05 and 0.5 m/s. The lower velocity represents very calm conditions, which are generally exceeded at dredging sites and in cases of silt curtain application (Jin et al., 2003; Vu et al., 2010; Spearman et al., 2011; De Wit et al., 2014), whereas flow velocities larger than 0.5 m/s also make silt curtains prone to mechanical failure (Francingues & Palermo, 2005).

Note that sediment settling is parameterized directly through the settling velocity, instead of through defining a particle diameter. Equivalent particle diameters corresponding to the values of w_s given in Table 1, assuming Stokes' law to apply to first order approximation, would range from 3 μm to 100 μm. Because silt curtains are used as an environmental mitigation measure to reduce spreading of fine sediment, there is no need to treat larger settling velocities or particle diameters. The tested values of w_s are sufficient to cover the range between very fine, persistent suspensions and flocculation conditions and are representative of suspended sediment properties in a dredge plume (Smith and Friedrichs, 2011).

The value of $C_{\max}$ is kept constant at 100 mg/L, which assures negligible influence of sediment concentrations on fluid density and does not induce hindered settling. This choice implies that the total amount of sediment introduced in the model may vary between the various simulations, as the sediment flux into the domain varies with the flow velocity. Simulation times are long enough to reach stationary conditions, so that time-averaged concentrations remain stable. Turbulence-averaged parameters are obtained for steady state conditions only.

Panel A of Figure 11 shows values of E_S at $10h_s$ downstream of the silt curtain as a function of h_{rel} and θ for initially uniform concentration profile 1 (e.g. for $h_{rel} = 0.5$, $U = 0.1$ m/s, $w_s = 1$ mm/s and $\theta = 10^{-2}$, a value of 12% is found for E_S at $x = 10h_s$). E_S appears to be very sensitive to changes in the velocity ratio θ. High settling velocities and low ambient flow velocities enhance the downward flux of suspended sediment between the upstream and downstream positions. A minor sensitivity of E_S to h_{rel} is found. Increasing the silt curtain height has a slightly unfavorable influence on the gross efficiency. Only for fairly high values of θ (e.g. $w_s = 5$ mm/s, $U = 10$ cm/s and $\theta = 5 \cdot 10^{-2}$) significant reduction of E_S is achieved. However, in most cases of silt curtain application, much lower settling velocities and higher ambient flow velocities are encountered (e.g. Jin et al., 2003 and Vu et al., 2010).

In panel B of Figure 11, values of E_{net} are given for upstream concentration profile 1. All deviations with respect to panel A are attributed to the different choice of efficiency parameter, which now excludes the effect of undisturbed settling. The diagram of E_S showed increasingly favorable values for high θ, whereas this trend has completely vanished in the diagram of E_{net}. Apparently flow separation and associated turbulent mixing caused by the silt curtain has a stronger effect than the initial downward flux induced by the curtain. The favorable gross efficiency for high θ is completely caused by autonomous settling. For low velocity ratios, corresponding to relatively fine sediment and high ambient flow velocities, no significant difference is found between both efficiency parameters as undisturbed settling is not important. The slightly favorable efficiency percentages for low h_{rel} around $\theta = 10^{-2}$ are not sufficient to achieve a reasonable reduction of the environmental impact potential and are again constrained to rather exceptional values of w_s and U.

Both right panels of Figure 11 present E_S (panel C) and E_{net} (panel D) for simulations with upstream concentration profile 2 (see Figure 10). As this profile contains all sediment in the upper half of the water column, curtain-induced turbulence may have a favorable influence through downward mixing of sediment. This favorable influence is indeed expressed by positive and increasing efficiency parameters as h_{rel} increases, while θ remains low. Silt curtains blocking a bigger part of the water column induce more intense mixing. However, again this favorable picture for E_S completely vanishes if results are expressed in terms of E_{net}, except for some negligibly small percentages (< 13%) in two regions of the diagram. Also for inflowing profiles of type 2, undisturbed settling leads to a higher efficiency than can be achieved with a silt curtain.

Discussion

Our results suggest that hanging silt curtains in a cross current cannot be effective in mitigating environmental impacts when assessed in a laterally homogeneous approach (i.e. effectively two-dimensional vertical), where horizontal diversion of currents around the curtain's edges is not possible. The downward flux of sediment induced by the curtain is compensated by intensified turbulent mixing. Such enhanced mixing will always occur when deploying a hanging silt curtain in ambient flow. At best, this leads to an approximately neutral effect of the silt curtain at high ambient flow velocities and low settling velocities of the sediment. Favorable settling conditions are obtained for low U and high w_s. These conditions are controlled by rapid settling of the sediment. Silt curtains then have an explicitly unfavorable influence. Vu and Tan (2013) have concluded that the relative curtain height is one of the main parameters controlling the flow field around a silt curtain. They suggest that optimizing the curtain height might lead to favorable efficiency of a silt curtain. Based on the results presented in the previous sections, we endorse the big sensitivity of the flow field to the relative silt curtain height. However, evaluation of E_{net} for the whole range of θ and h_{rel} encountered in practice (panels B and D of Figure 11) leads to the conclusion that an optimal curtain height with favorable silt curtain efficiency does not exist. These findings do absolutely not imply that doing nothing is a viable strategy, as this may result in a significant environmental impact at some distance of a dredging site. PIANC (2010) have promoted the use of adaptive management strategies for environmental mitigation to cope with the site-specific and unpredictable nature of dredging projects.

In reality, silt curtains have a finite width, and the flow can pass around their edges. Possible configurations in the horizontal plane have been shown in Figure 2. When applied in an open configuration (i.e. (a) in Figure 2), lateral boundaries are absent. Hence a three-dimensional flow field will develop, consisting of both vertical flow diversion (passing underneath) and horizontal flow diversion (passing around the edges). However, vertical diversion of the sediment-laden flow is still the intended working principle of a silt curtain. If the current is diverted horizontally, part of the suspended sediment will leak away without being brought closer to the bed by the curtain. Furthermore, additional flow separation and turbulent mixing is induced in the horizontal plane. Hence, the possibility of horizontal diversion is expected to result in decreased efficiency of hanging silt curtains. The question remains which portion of upstream suspended sediment will be diverted horizontally. Radermacher et al. (2013) have used two-dimensional horizontal (2DH) model simulations to assess the distribution of the upstream water discharge over vertical and horizontal diversion, incorporating the silt curtain as an internal discharge condition. For realistic values of F and relative curtain width W_{rel} (i.e. F larger than 0.01 and W_{rel}, being the curtain width divided by the water depth, smaller than 100), they found that the fraction of the upstream discharge being diverted around the edges of the curtain is about equal to the relative curtain height. A silt curtain covering 60% of the water column causes about 60% of the upstream water to pass the curtain around its edges and about 40% to pass underneath the curtain. Although their 2DH, Reynolds-averaged modeling approach and assessment of discharges rather than sediment fluxes has its limitations, the results of Radermacher et al. (2013) can be used as a first order approximation of the effect of horizontal diversion. As a result, the efficiency percentages derived from Figure 11 are expected to be an upper limit, applying to the most favorable case of an infinitely wide silt curtain without horizontal diversion. Furthermore, these results imply that deployment of silt curtains with high values of h_{rel} (or even covering the full water depth, such as the standing silt curtains that were mentioned in the introduction) leads to strong horizontal diversion of the flow, leaving the vertical distribution of suspended sediment in the water column largely untouched. If the curtain would be used in the near vicinity of the sensitive receptor, horizontal diversion may have a favorable effect by guiding suspended sediment away from the sensitive environment. However, in that case, partial vertical diversion and horizontal mixing through lateral shear downstream of the edges of the curtain will decrease silt curtain efficiency. The creation of a (spatially limited) calm zone just upstream of the curtain in case of large horizontal diversion might be another potential working mechanism of hanging silt curtains.

The influence of waves and wind-driven currents has been omitted in this study. Unlike currents, waves do not have the potential to transport suspended sediment over considerable distances. Their influence is therefore limited to potential destabilization of the curtain, enhancing curtain-induced turbulence. Wind-driven currents would produce an upstream flow profile different from the logarithmic profile used here. If the current is fully developed, or if an additional forcing mechanism is present (e.g. tide, free surface gradient), the full discharge will still pass underneath the curtain. Strong vertical redistribution of momentum in the contracting and separating flow past the silt curtain makes the downstream flow field practically insensitive to the upstream velocity profile. The only exception would be the case of not fully developed, purely wind-driven currents, where the flow in the top layer might be compensated by a curtain-induced return current near the bed. It is stressed that additional forcing mechanisms, other than wind, are very often present in a marine or riverine environment.

The sediment concentration profiles that were used in the numerical model simulations as an upstream boundary condition are highly schematic. Several other profiles have been tested in this study as well, including profiles which vary linearly over depth, and an empirical Rouse-like profile corresponding to suspended fine sediment in equilibrium conditions (Whitehouse et al. 2000). However, concentration profiles encountered near a silt curtain are usually still fairly close to the source of suspended sediment. The range of realistic profiles is therefore very wide and is not constricted to equilibrium conditions. The two profiles presented in this paper can be thought to represent the two extreme cases that might potentially yield favorable silt curtain efficiency. Profile 1 has no vertical gradients and therefore allows a minimum amount of curtain-induced diffusion. Profile 2 contains all suspended sediment near the free surface, where it contributes maximally to the environmental impact potential (P). Sediment can only be transported to a lower level in the water column, which by definition leads to a decrease in P. Hence, this provides an opportunity to the silt curtain to achieve favorable efficiency by vertical mixing. However, net silt curtain efficiency is still unfavorable for profiles 1 and 2, which further supports the conclusions drawn from this study.

Furthermore, we have used a single sediment fraction, i.e. a single value of w_s that applies to a single model simulation. We have limited our study to conditions which do not involve hindered settling (see e.g. Whitehouse et al., 2000), so non-linear interactions between different sediment fractions can be neglected. As a result, the effect of multiple sediment fractions can be determined by evaluating the efficiency parameters separately for every fraction.

One aspect that has not been mentioned before is the increase in bed shear stresses caused by a hanging silt curtain, induced by high near-bed velocities and increased turbulence intensities. It is expected that this would enhance erosion of the bed, adding to the turbidity in the water column and reducing the curtain's efficiency even further. However, this is only an initial effect, as a new equilibrium between enhanced bed shear stresses and bed stability will develop.

Conclusions

We have modeled the efficiency of hanging silt curtains, considering vertical diversion of the sediment-laden current to be the main working principle. Use was made of Large Eddy Simulation to compute efficiency percentages in a two-dimensional vertical framework with the silt curtain spanning the full width of the model. Validation of the numerical model was done by means of laboratory experiments. The LES model was shown to be capable of accurately predicting vertical diversion of flow past a hanging silt curtain, in terms of time-averaged flow velocities and turbulence parameters. The tested range of relevant input parameter values was selected to be representative of typical cases of silt curtain application.

In order to compute the efficiency, a new parameter was introduced. The commonly used gross efficiency parameter cannot be a suitable measure in case of favorable settling conditions (low ambient flow velocity and high settling velocity). Instead, we propose a net efficiency parameter, which compares silt curtain performance to a reference situation without such a curtain. The region over which silt curtain efficiency is evaluated ranges from upstream of the curtain to well beyond the recirculation zone at the downstream side, which approximately captures the region over which the fluid flow is affected by the presence of the silt curtain. Hanging silt curtains were shown to be an ineffective environmental measure for mitigation of suspended sediment concentrations when applied in cross-flow. An initial, downward flux of sediment is induced by the silt curtain, but is counteracted by curtain-induced flow separation and associated increased turbulent mixing. In case of favorable settling conditions, undisturbed settling of the sediment without a silt curtain is more effective than settling with a silt curtain in place. Thus under such conditions, the use of silt curtains leads to a larger environmental impact around a dredging site than without a silt curtain. In case of unfavorable settling conditions (high ambient flow velocity and low settling velocity), the silt curtain hardly has an influence. The height of the silt curtain relative to the water depth determines the amount of disturbance of the flow. A relatively deep curtain, blocking a larger part of the water column, leads to stronger turbulent mixing. Generally this yields unfavorable effects. Only when the sediment concentration profile at the upstream side of a silt curtain is biased towards the upper half of the water column and settling conditions are favorable, a higher silt curtain may lead to a slightly more favorable, but still negligible efficiency. In summary, no possibilities for efficiently applying a hanging silt curtain in cross-flow were found, considering vertical diversion of the sediment-laden current to be the main working principle.

It should however be noted that doing nothing is not a viable alternative for silt curtain application. Decisions on mitigation of possible environmental impact should always be based on a site-specific analysis, taking into account the local variability of environmental conditions and the dredging activities concerned.

It is recommended to use the findings presented in this paper to optimize the design of future field experiments with respect to silt curtain efficiency. Although the processes governing silt curtain efficiency have been studied extensively in a numerical modeling environment, it is important that these processes are identified and quantified in the field as well. Furthermore, this will yield more insight in possible complicating factors like wave motions and wind-driven currents.

Acknowledgements

This research was initiated and partly facilitated by dredging company Boskalis, in particular by Fokko van der Goot, Stefan Aarninkhof, Gerard Hoogewerff and Karoune Nipius. They are greatly acknowledged for backing up the simulation results with field experience and knowledge on marine ecology. Svasek Hydraulics is acknowledged for its share in the numerical model simulations. Finally, the laboratory staff of the TU Delft Laboratory for Fluid Mechanics is thanked for facilitating the physical model study.

Notation

C = Suspended sediment concentration [kg/m^3];

$C_{\max}$ = Maximum C in upstream domain [kg/m^3];

C_s = Constant in sub-grid model [kg/m^3];

C_* = Dimensionless C [-];

E_{net} = Net silt curtain efficiency [%];

E_S = Gross silt curtain efficiency [%];

E_{ref} = Reference efficiency [%];

E_{zz} = Spectral density of turbulent kinetic energy [m^2/s^2/Hz];

F = Froude number [-];

P = Environmental impact potential [-];

P_{in} = P at inflow boundary [-];

P_{ref} = P in reference situation [-];

R = Reynolds number [-];

Sc = Turbulent Prandtl-Schmidt number [-];

U = Depth-averaged flow velocity [m/s];

W_{rel} = Relative silt curtain width [m/s];

f = Frequency [s^{-1}];

$\mathbf{f}$ = Acceleration vector due to body forces [m/s^2];

g = Gravitational acceleration [m/s^2];

h = Water depth [m];

h_{rel} = Relative silt curtain height [-];

h_s = Silt curtain height [m];

p = Pressure [kg/(s^{2}m)];

r_u = Turbulence intensity of u-velocity [m/s];

r_w = Turbulence intensity of w-velocity [m/s];

t = Time [s];

$\mathbf{u}$ = Velocity vector [m/s];

$\bar{u}$ = Time-averaged velocity in x-direction [m/s];

$\bar{w}$ = Time-averaged velocity in z-direction [m/s];

w_s = Settling velocity [m/s];

x = x-coordinate [m];

y = y-coordinate [m];

z = z-coordinate [m/s];

z_* = Dimensionless *z*-coordinate [-];

Γ = Diffusion coefficient [m^2/s];

θ = Velocity ratio [-];

ν = Kinematic viscosity [m^2/s];

ν_e = Eddy viscosit [m^2/s];

ν_{mol} = Molecular viscosity [m^2/s];

ν_{sgs} = Sub-grid-scale viscosity [m^2/s];

ν_t = Turbulent viscosity [m^2/s];

ρ = Density [kg/m^3];

ρ_s = Sediment density [kg/m^3];

ρ_a = Ambient water density [kg/m^3];

$\boldsymbol{\tau}$ = Shear stress tensor [kg/(s^{2}m)]; and

τ_{uw} = Reynolds shear stress in the x-z plane [kg/(s^{2}m)].

References

Antonopoulos-Domis M. (1981). "Large-eddy simulation of a passive scalar in isotropic turbulence." *Journal of Fluid Mechanics*, 104, 55-79.

Bray R.N. – editor (2008). *Environmental aspects of dredging*, Taylor & Francis, Leiden, Netherlands.

Erftemeijer P.L.A. and R.R. Robin Lewis (2006). "Environmental impacts of dredging on seagrasses: a review." *Marine Pollution Bulletin*, 52(12), 1553-1572.

Erftemeijer P.L.A., B. Riegl, B.W. Hoeksema and P.A. Todd (2012). "Environmental impact of dredging and other sediment disturbances on corals: a review." *Marine Pollution Bulletin*, 64 (9), 1737-1765.

Fadlun, E., Verzicco, R., Orlandi, P., Mohd-Yusof, J. (2000). "Combined immersed-boundary finite-difference methods for three-dimensional complex flow simulations." *Journal of Computational Physics*, 161(1), 35-60.

Francingues N.R. and M.R. Palermo (2005). "Silt curtains as a dredging project management practice." *DOER Technical Notes Collection (ERDC TN-DOER-E21)*, U.S. Army Engineer Research and Development Center, Vicksburg, USA.

Jarrin, N., S. Benhamadouche, D. Laurence and R. Prosser (2006). “A synthetic-eddy-method for generating inflow conditions for large-eddy simulations.” *International Journal of Heat and Fluid Flow*, 27(4), 585-593.

JBF Scientific Corporation (1978). “An analysis of the functional capabilities and performance of silt curtains.” *Technical Report D-78-39*, U.S. Army Engineer Waterways Experiment Station, Vicksburg, USA.

Jin J.Y., J.W. Chae, W.O. Song, J.S. Park, S.E. Kim, W.M. Jeong, K.D. Kum and J.K. Oh (2003). “Behavior of currents and suspended sediments around a silt screen.” *Ocean and Polar Research*, 25(3S), 399-408.

Kraichnan R.H. and D. Montgomery (1980). “Two-dimensional turbulence.” *Reports on Progress in Physics*, 43, 547-619.

Manninen, M., Taivassalo, V., Kallio, S. (1996). “On the mixture model dredger: the effect of dredging speed, propeller, overflow location for multiphase flow.” *VTT publications 288*, Technical Research Center of Finland.

Nicoud, F. and F. Ducros (1999). “Subgrid-scale stress modeling based on the square of the velocity tensor.” *Flow, turbulence and combustion*, 62, 183-200.

Ogilvie J.C., D. Middlemiss, M.W. Lee, N. Crossouard and N. Feates (2012). “Silt curtains – a review of their role in dredging projects.” *Proc., CEDA Dredging Days*, Abu Dhabi, UAE.

PIANC (2010). “Dredging and port construction around coral reefs.” *PIANC report no. 108 – 2010*.

Pope, S.B. (2000). *Turbulent Flows*, Cambridge University Press, Cambridge, UK.

Radermacher M., F. van der Goot, D.C. Rijks and L. de Wit (2013). “The art of screening: efficiency of silt screens.” *Proc., World Dredging Congress XX*, Brussels, Belgium.

Smith, S.J. and C.T. Friedrichs (2011). “Size and settling velocities of cohesive flocs and suspended sediment aggregates in a trailing suction hopper dredge plume.” *Continental Shelf Research*, 31(10), S50-S63.

Spearman, J., A. de Heer, S. Aarninkhof and M. van Koningsveld (2011). “Validation of the TASS system for predicting the environmental effects of trailing suction hopper dredgers.” *Terra et Aqua*, 125, 14-22.

Van Prooijen, B.C. and J.C. Winterwerp (2010). “A stochastic formulation for erosion of cohesive sediments.” *Journal of Geophysical Research*, 115(C1), C01005.

Vu, T.T. and S.K. Tan (2010). “Laboratory investigation of hydraulic performance of silt screens.” *Proc., 9th International Conference on Hydrodynamics*, Shanghai, China.

Vu, T.T., S.K. Tan and S. Doorn-Groen (2010). “A case study of silt screen performance.” *Proc., World Dredging Congress XIX*, Beijing, China.

Vu, T.T. and S.K. Tan (2013). “Velocity and turbulence characteristics around a silt screen.” *Maritime Engineering*, 166(2), 89-97.

Wang, H., F. Si, G. Lou, W. Yang and G. Yu (2015). “Hydrodynamic characteristics of a suspended curtain for sediment trapping.” *Journal of Waterway, Port, Coastal and Ocean Engineering*, 141(1), 04014030.

Whitehouse, R.J.S., R.L. Soulsby, W. Roberts and H.J. Mitchener (2000). *Dynamics of estuarine muds*, Thomas Telford Publishing, London, UK.

Wit, L. de and C. van Rhee (2012). “Testing different advection schemes for coarse high Re LES simulations of jet in crossflow and coflow.” *Proc., 9th International ERCOFTAC Symposium on Engineering Turbulence Modelling and Measurements*, Thessaloniki, Greece.

Wit, L. de, A.M. Talmon and C. van Rhee (2014). “3D CFD simulations of trailing suction hopper dredger plume mixing: Comparison with field measurements.” *Marine Pollution Bulletin*, 88, 34-46.

Wit, L. de (2015). *3D CFD modelling of overflow dredging plumes*, PhD thesis, Delft University of Technology.

Yasui A., I. Deguchi and M. Ono (1999). “Performance of silt protector in three dimensional flow.” *Proc., Ninth International Offshore and Polar Engineering Conference*, Brest, France.

Appendix. Numerical model description

In the CFD model the Navier Stokes equations with variable density are solved, see Equations 8 and 9.

$$\frac{\partial \rho}{\partial t} + \nabla \cdot \left(\rho \mathbf{u} \right) = 0 \tag{8}$$

$$\frac{\partial \rho \mathbf{u}}{\partial t} + \nabla \cdot \left(\rho \mathbf{u}\mathbf{u} \right) = -\nabla p + \nabla \cdot \boldsymbol{\tau} + \rho \mathbf{f} \tag{9}$$

where ρ is the density, $\mathbf{u}$ is the velocity vector, p is the pressure, $\boldsymbol{\tau}$ is a shear stress tensor and $\mathbf{f}$ is the acceleration vector due to body forces. The shear stress tensor $\boldsymbol{\tau} = \nu_e \left(\nabla \mathbf{u} + \nabla \mathbf{u}^T - 2/3 \nabla \cdot \mathbf{u} \right)$ contains a contribution from molecular and turbulent viscosity by the eddy viscosity concept: $\nu_e = \nu_{mol} + \nu_t$. Turbulence is modelled using the LES approach in which a spatial filter equal to the mesh size is applied to the flow field and a turbulence model is used for the sub-grid-scale contribution: $\nu_t = \nu_{sgs}$. This sub-grid-scale viscosity is determined by the WALE model (Nicoud and Ducros 1999) with Smagorinksy constant $C_s = 0.325$. The sediment volume concentration C is resolved with Equation 10.

$$\frac{\partial C}{\partial t} + \nabla \cdot \left(\mathbf{u} C \right) = \nabla \cdot \left(\Gamma \nabla C \right) \tag{10}$$

with the diffusion coefficient $\Gamma = \nu_e / \sigma_T$ and a turbulent Prandtl-Schmidt number $Sc = 0.5$. The density ρ is obtained from the sediment concentration by Equation 11.

$$\rho = \rho_a + (\rho_s - \rho_a) C \tag{11}$$

where ρ is the actual mixture density at each location in the grid, ρ_s is the sediment density and ρ_a is the ambient water density. A second order (time and space) parallel (domain decomposition) finite volume method is used on a staggered mesh. Advection of momentum is carried out with a low dissipation artificial viscosity scheme AV6 to prevent wiggles in front of the silt curtain (De Wit and Van Rhee 2012). Advection of sediment concentration is carried out with a Total Variation Diminishing (TVD) scheme with the Van Leer limiter to prevent non-physical negative concentrations. The silt curtain is implemented using a direct forcing Immersed Boundary Method (Fadlun et al. 2000).

Sediment particles settle with gravity with a vertical drift velocity superimposed on the CFD flow velocity (Manninen et al. 1996). At the bed, sediment particles deposit with the settling velocity. Erosion from the bed of previously deposited sediment is not accounted for in the simulations. For more details about the CFD model, see De Wit (2015).

Table 1. Ranges of tested parameter values in the numerical model.

Parameter	Range
U	0.05 – 0.5 [m/s]
w_s	0.01 – 10 [mm/s]
h_s	1.25 – 3.75 [m]
H	5.0 [m]

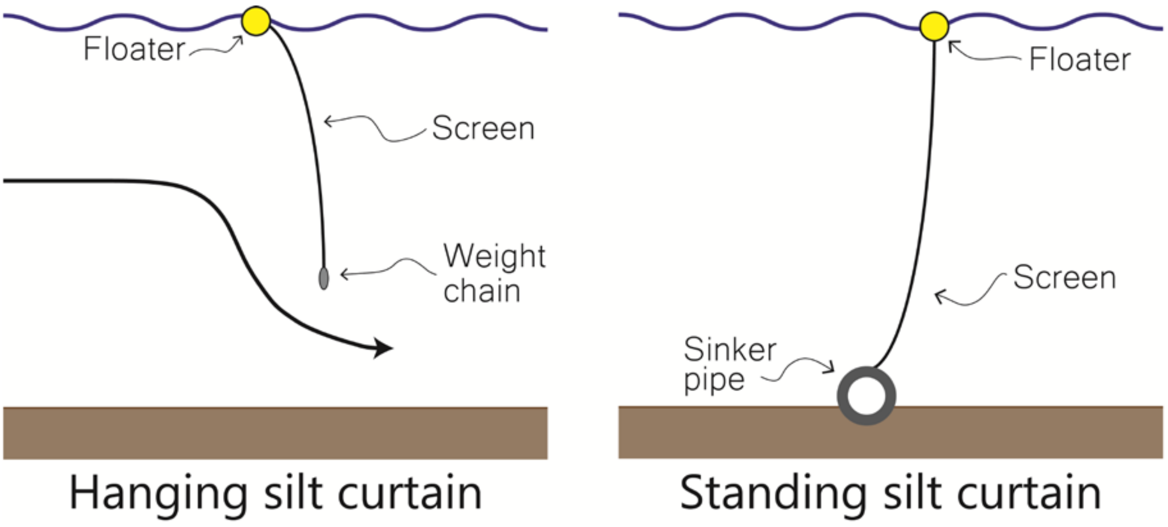

Fig. 1. Schematic cross-section of silt curtain types: hanging (left) and standing (right).

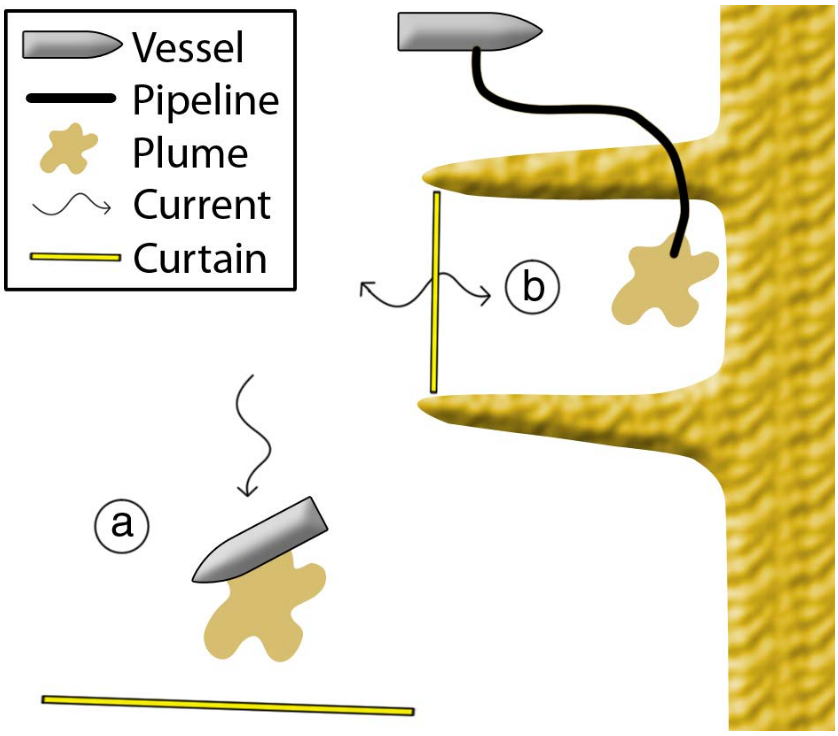

Fig. 2. Typical configurations of hanging silt curtains in the horizontal plane: (a) open configuration and (b) near a semi-enclosed reclamation area.

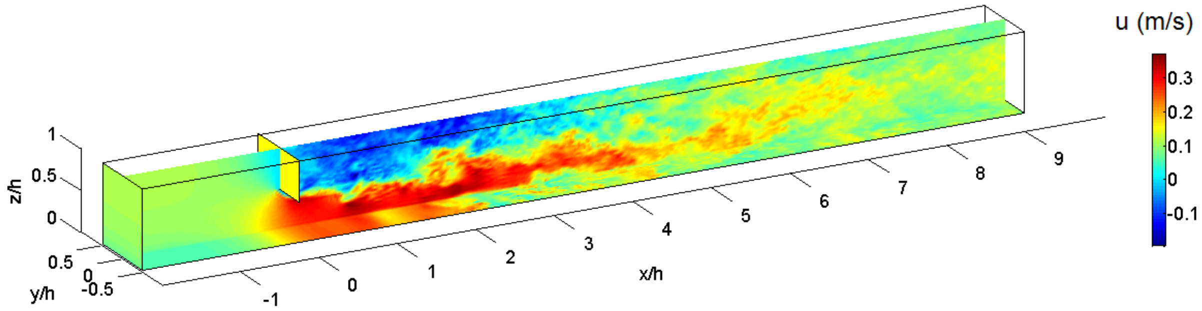

Fig. 3. Geometry of the numerical model domain. The hanging silt curtain is depicted as a vertical plane at $x = 0$. For simulations at laboratory scale, h equals 0.35 m, whereas this is 5 m in real scale simulations. The nature of LES is clearly demonstrated by the turbulent eddies present in the plot of horizontal velocities during an arbitrary simulation.

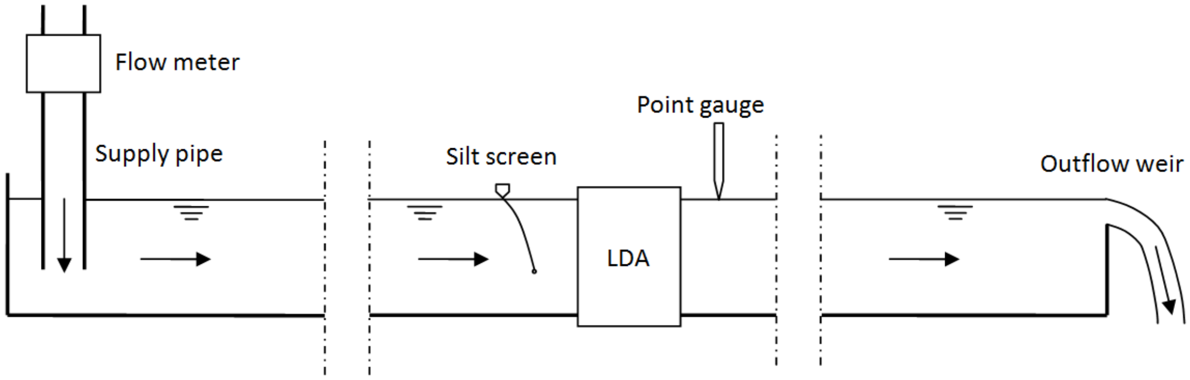

Fig. 4. Schematic diagram of the experimental setup in the laboratory flume with a total length of 14 m.

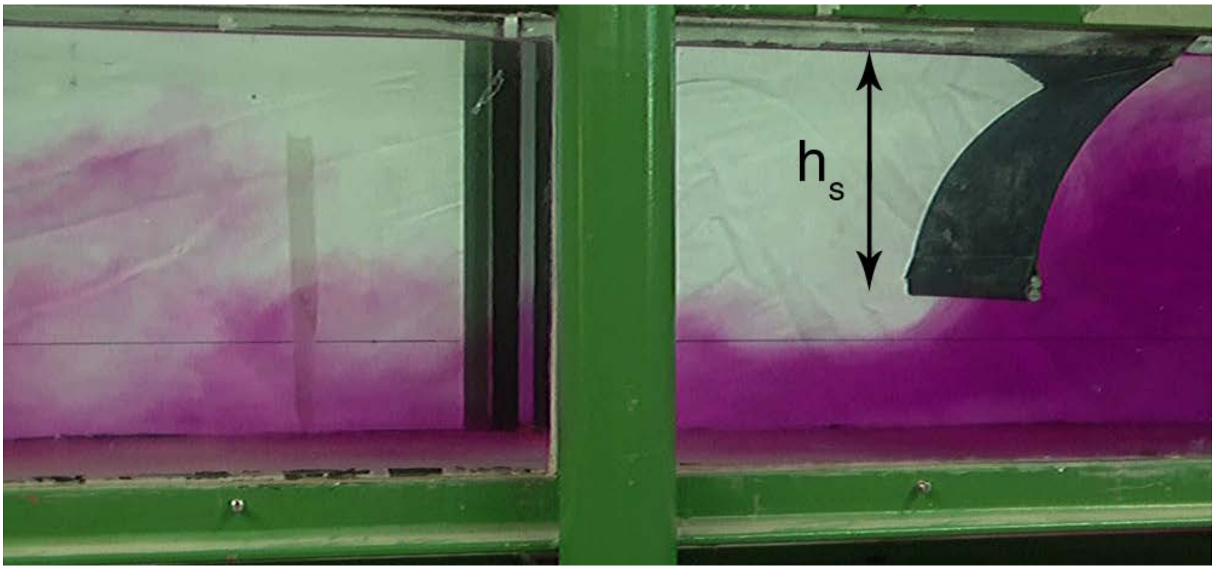

Fig. 5. Snapshot of a dye injection in the laboratory flume, during an experiment with $Fr = 0.043$ and $h_{rel} = 0.75$ (before flaring). Image by Max Radermacher.

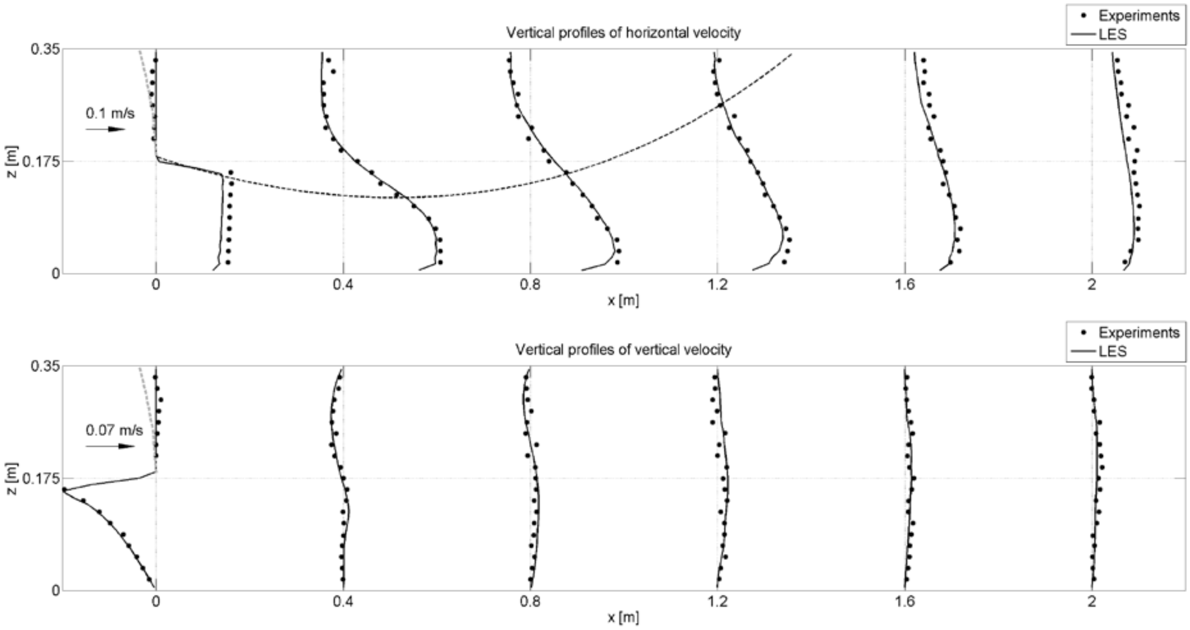

Fig. 6. Measured and computed time-averaged flow velocities $\overline{u}$ and $\overline{w}$. The laboratory measurements are represented by dots, the LES results by solid lines. The arrow at the left indicates the scale of the velocity axis at each vertical profile. The dashed gray line shows the deformation of the silt curtain during the laboratory run. The approximate extent of the recirculation zone in the wake of the silt curtain is indicated with a black dashed line in the upper panel.

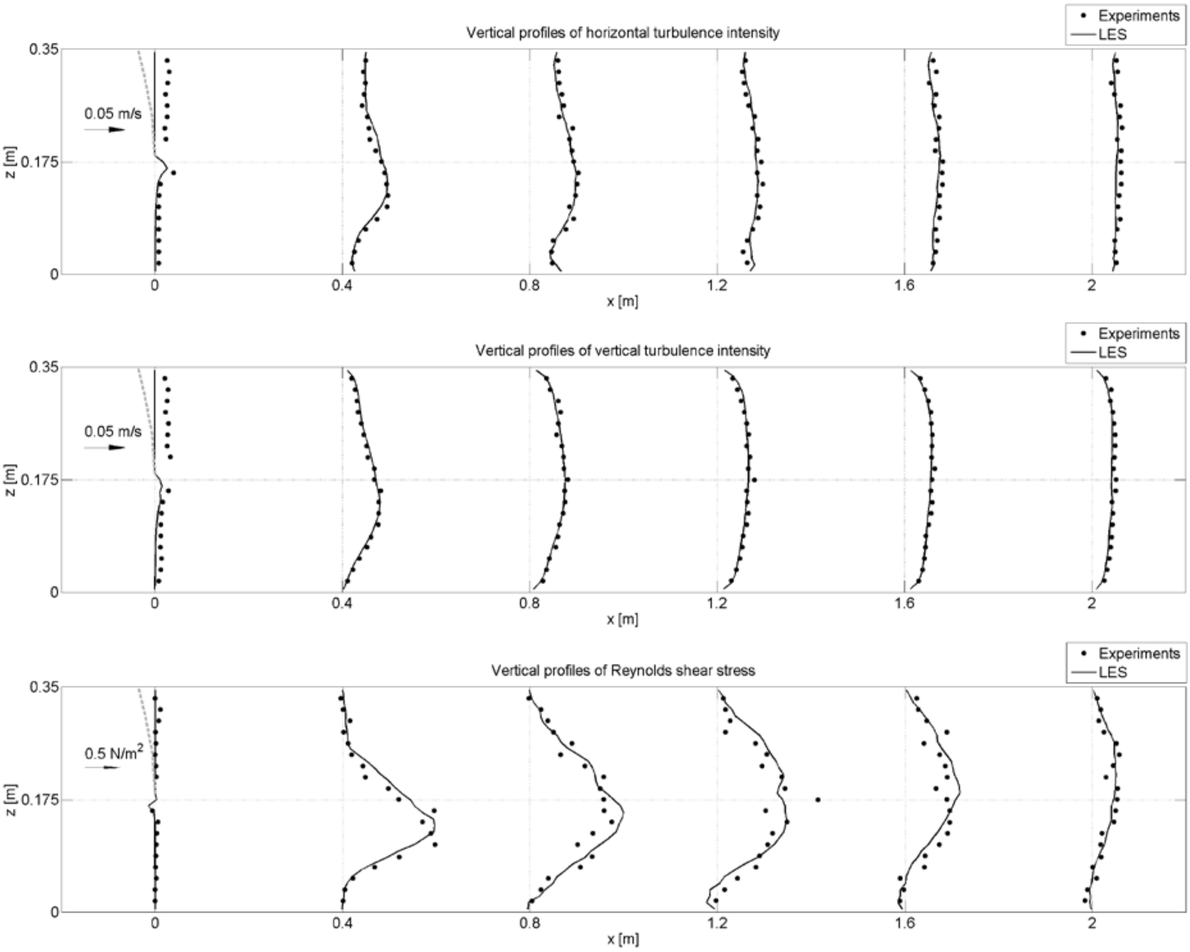

Fig. 7. Measured and computed turbulence parameters: turbulence intensities r_u and r_w and Reynolds shear stress τ_{uw}.

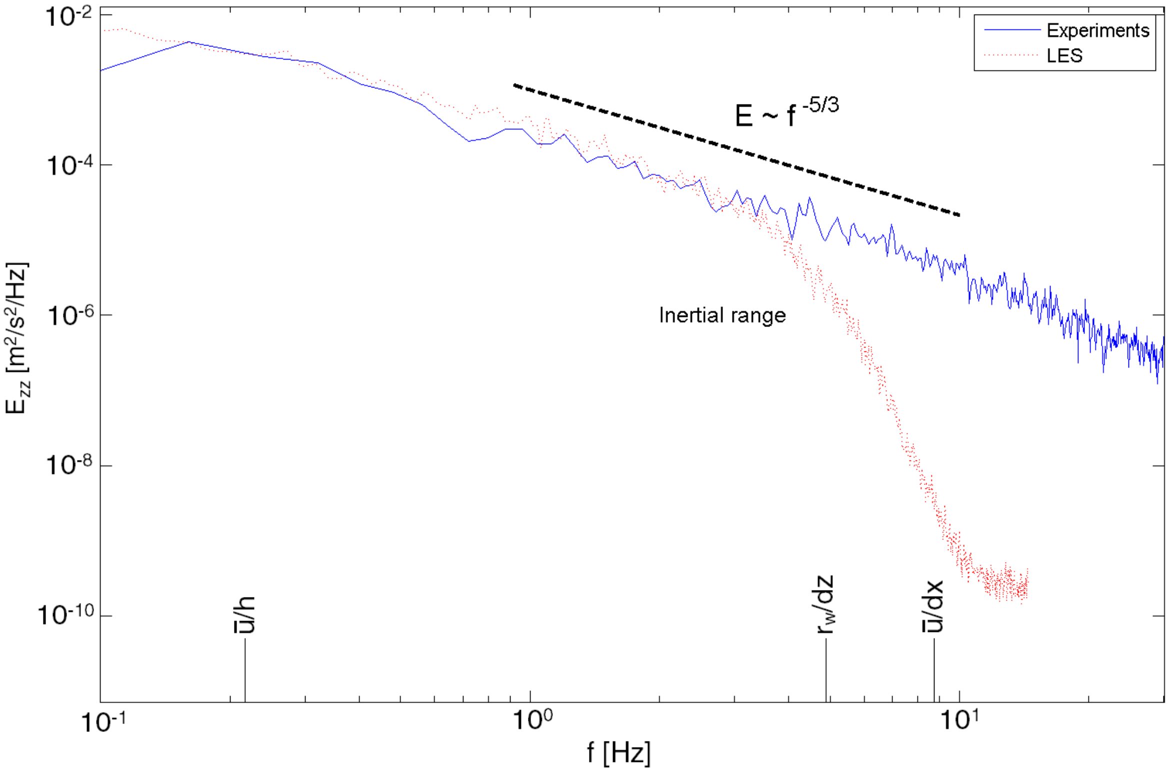

Fig. 8. Turbulent kinetic energy density spectra for a laboratory time series of vertical velocity w and its numerical counterpart. Several characteristic time scales are indicated along the frequency axis: $\overline{u}/h$ is a measure for the lowest turbulent frequencies that can occur in the model domain, whereas $\overline{u}/dx$ (with dx the mesh size in x direction) is a measure for the highest turbulent frequencies that can be computed on the numerical grid and r_w/dz is a measure for the frequency where the sub-grid-stress model comes into play.

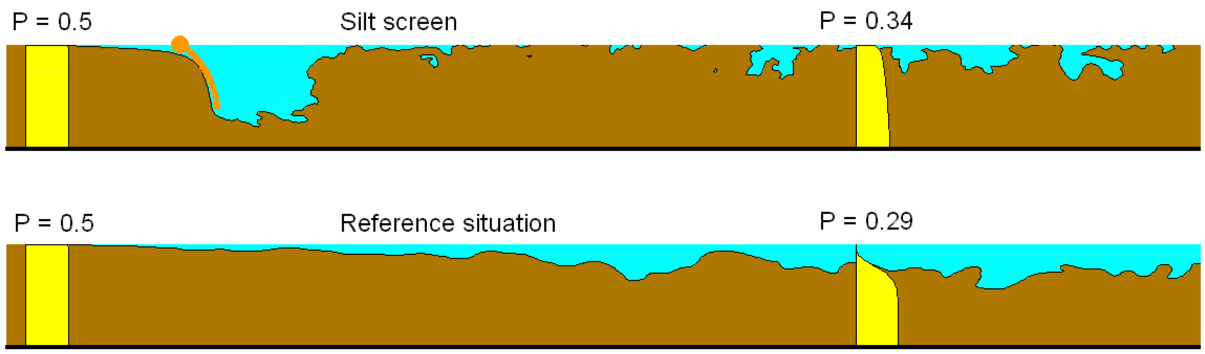

Fig. 9. Schematic example of vertical profiles of $C_* z_*$ for a situation with and without a silt curtain. The depth-integrated value (i.e. P) is indicated above each profile. In this particular example, application of a silt curtain is unfavorable, as $E_S = 32\%$ and $E_{net} = -10\%$, i.e. a deterioration of turbidity levels.

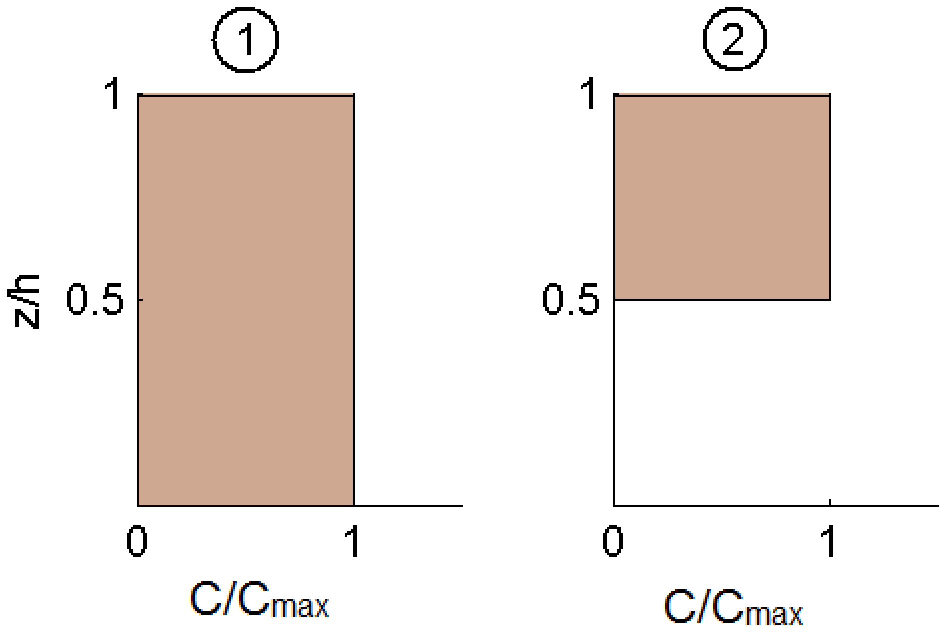

Fig. 10. Different concentration profiles 1 and 2 as applied at the upstream boundary in the numerical model simulations.

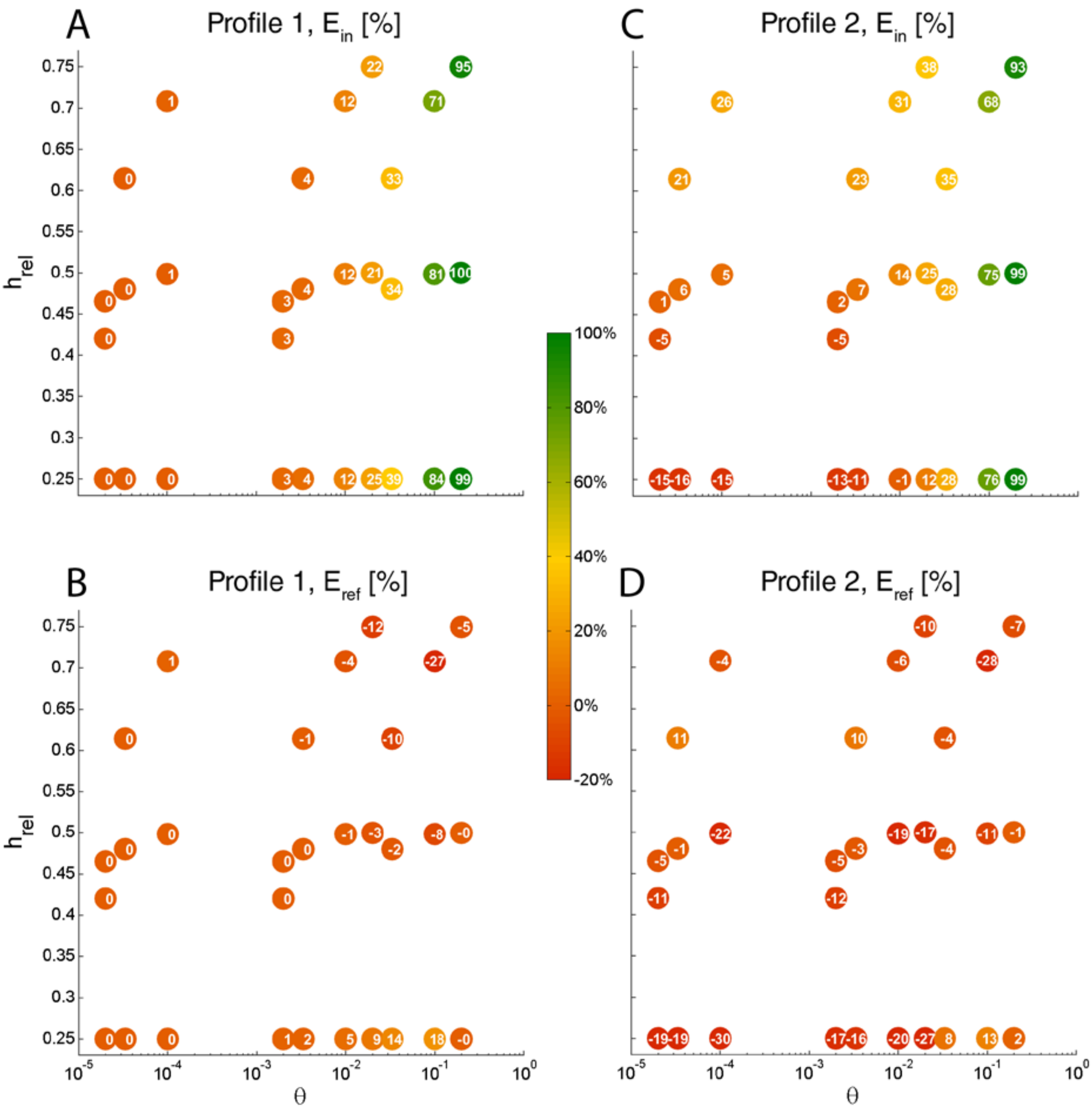

Fig. 11. Results of the numerical simulations as a function of θ and h_{rel}. Coloured dots in the upper panels (A & C) represent inflow efficiency $E_S\left(10h_s\right)$, those in the lower panels (B & D) represent $E_{net}\left(10h_s\right)$. The results in the left panels (A & B) are obtained from simulations with inflow profile 1, those in the right panels (C & D) are obtained from simulations with inflow profile 2. The numbers in the dots show the exact efficiency percentage obtained from every model simulation.